Radiance Distribution Measurements in Coastal Water

Kenneth J. Voss

Institute of Marine Resources, Scripps Institution of Oceanography, UCSD
La Jolla, CA 92093-0218

ABSTRACT

A new instrument for measuring the underwater spectral radiance distribution has been built. This instrument, an electro-optic radiance distribution camera system (RADS), allows a complete spectral radiance distribution to be measured in a short period of time and the reduction of these data to absolute radiometric values as a routine procedure. Data taken with the RADS system at various depths will be presented. These data will be reduced to obtain various apparent optical properties such as scalar irradiance, vector irradiance, and average cosine. Also, the radiance attenuation coefficient will be discussed as derived from the radiance distribution data.

1. INTRODUCTION

The radiance distribution contains the most complete set of apparent optical parameters which can be measured. However, in the past it has been difficult and time consuming to make these measurements, and therefore not many have been made. Because of the completeness of the measurement, the radiance distribution can be used to obtain not only scalar irradiance, vector irradiance, and apparent optical properties such as the diffuse attenuation coefficient, and reflectance; but it is also theoretically possible to derive the inherent optical properties of volume scattering function and the absorption coefficient from the variation of the radiance distribution with depth.

The electro-optic radiance distribution camera system (RADS)[1] has been used to obtain radiance distribution data, during a cruise off of San Diego, California. In this paper, data taken with the RADS system at various depths, during this cruise, will be presented. These data will be reduced to obtain various apparent optical properties such as scalar irradiance, vector irradiance, and average cosine. Also, the radiance attenuation coefficient will be discussed and then obtained from the radiance distribution data.

2. RADIANCE DISTRIBUTION THEORY

Radiance is defined as the radiant flux per unit solid angle per unit projected area from a given direction; whereas the spectral radiance distribution is the collection of radiance data for all directions at a given point in space at a certain wavelength.[2] As has been illustrated elsewhere,[1,3] all other apparent optical properties can be derived from a collection of radiance distribution measurements. Figure 1 illustrates how the radiance distribution fits into the overall scheme of apparent and inherent optical properties and is a central measurement of ocean optical properties.

The radiance distribution can also be used to solve other problems in radiative transfer theory. One example of this is the apparent contrast reduction, an important problem in underwater visibility and imaging. Preisendorfer[4] derived the general case of the inherent contrast of an object in a medium to be:

$$C_r = C_0 \exp\left(-\int_{\zeta(r,\theta,\varphi)} (c - \zeta(r,\theta,\varphi) \cdot \mathbf{K}(r,\theta,\varphi))dr'\right), \quad (1)$$

where C_0 is the inherent contrast of the object, defined by:

$$C_O = (L_t - L_b)/L_b. \tag{2}$$

L_t is the target radiance, L_b is the background radiance, $\zeta(r,\theta,\varphi)$ is the direction of the path, c is the beam attenuation and $\mathbf{K}(r,\theta,\varphi)$ is the radiance attenuation function defined by:

$$\mathbf{K}(r,\theta,\varphi) = -(1/L(z,\theta,\varphi))\,\nabla L(z,\theta,\varphi). \tag{3}$$

A common assumption in ocean optics is that the ocean in the neighborhood of the measurement is a stratified plane-parallel medium. With this simplification, the gradient of $L(z,\theta,\varphi)$ in the x and y directions are zero and the expression for the radiance attenuation function reduces to:

$$\mathbf{K}(r,\theta,\varphi) = -(1/L(z,\theta,\varphi))\,dL(z,\theta,\varphi)/dz\,\mathbf{k}, \tag{4}$$

where $\mathbf{k}$ is the unit vector in the z direction. In this case, the expression for the apparent contrast reduces to:

$$C_r = C_O \exp\left(-\int_{\zeta(r,\theta,\varphi)} (c+K(r,\theta,\varphi)\cos(\theta))dr\right) \tag{5}$$

where $\cos(\theta)$ is the angle between the zenith and the path ($K(r,\theta,\varphi) = |\mathbf{K}(r,\theta,\varphi)|$).

This function, $K(r,\theta,\varphi)$, takes on special meaning in the case of the upwelling radiance distribution in an infinitely deep medium (or for positions in the medium at which the bottom reflectance does not affect the light field). The general equation of transfer for radiance (in the plane parallel stratified medium) has been shown by Preisendorfer[5] to be of the form:

$$L(z,\theta,\varphi) = L_O(z,\theta,\varphi)\exp\left(-\int_{\zeta(r,\theta,\varphi)} cr\,dr'\right) + \tag{6}$$
$$\left(L^*\left(1-\exp\left(-\int_{\zeta(r,\theta,\varphi)}(c-K(r,\varphi,\theta)\cos(\theta))\,dr'\right)\right) / (c+K(r,\theta,\varphi)\cos(\varphi))\right.$$

When the above conditions are satisfied the path length can be taken to be infinity and the expression for the radiative transfer equation reduces to:

$$L(z,\theta,\varphi)) = L^*/(c+K(r,\theta,\varphi)\cos(\theta)) \tag{7}$$

and the radiance attenuation coefficient becomes:

$$K(r,\theta,\varphi) = -(1/L(z,\theta,\varphi))\,d(L^*/(c+K(r,\theta,\varphi)\cos(\theta)))/dz. \tag{8}$$

In this case it is easy to see that the $K(r,\theta,\varphi)$ is a function of the path radiance. As such, $K(r,\theta,\varphi)$ can be negative, implying an increase in radiance with depth for a given direction. This case was observed in the data in the direction of the shadow of the ship -- the radiance in this direction increased with depth, as the path length from the ship to the instrument increased.

At the asymptotic depth, the radiance distribution, as discussed by many authors,[4,6,7] no longer changes its shape but only decreases in magnitude. In this case $K(r,\theta,\varphi)= k$, a factor which is independent of direction. A test of whether the asymptotic radiance distribution, in an experimental situation, has been reached is to reduce $K(r,\theta,\varphi)$ from the radiance distribution data and determine the variation with angle; a single valued function would indicate that the asymptotic region has been reached.

3. EXPERIMENTAL DESIGN

The RADS camera system used to make these radiance distribution measurements has been described in detail elsewhere,[1] however a brief description will be included. The RADS system uses two cameras with fisheye lenses in a method similar to that of Smith et al.;[3] however, it has electro-optic charge injection device cameras (CID) rather than photographic cameras. This method has the advantages of the photographic method (use of imagery to store and process the data), but avoids the problems with photographic radiometry. Figure 2 shows a stylized block diagram of the instrument.

Plastic hemispherical domes were used as windows in this instrument. In the case of the downwelling radiance distribution window, a neutral density coating (1 optical density) was applied in the region between 0 and 48 degrees zenith angle. This region of the downwelling distribution can be assumed to be the brightest area in the underwater image ("manhole" effect[8]) in that all skylight will be refracted into this angular range at the air-water interface. The neutral density coating increased the effective intrascene dynamic range of the camera to over 3 orders of magnitude. A Bicar fisheye converter lens was used as the input to the optical train. The fisheye lens characteristically projects a 2π steradian hemisphere onto the film plane via an equidistant projection.[9] In this type of projection the zenith angle, θ, is projected onto the film plane through the equation:

$$r = f\,\theta \tag{9}$$

where f is the focal length of the lens and r is the radial distance from the center of the image plane.

A filter changer was designed to be inserted between the fisheye lens and the camera and was used to determine the camera systems spectral response. This filter changer allowed four spectral filters (interference filters with approximate bandpass of 25 nm, and centers at 450 nm, 500 nm, 550 nm, and 600 nm) and four absorption neutral density filters (to adjust the average intensity of the scene to the optimum for the camera) to be inserted into the optical path. These filter changers were controlled from the surface enabling measurement with multiple spectral ranges during a single hydrocast. The resultant optical system measured the radiance distribution from 0 degrees zenith to 87.5 degrees zenith for the downwelling radiance distribution, and 92.5 degrees to 180 degrees for the upwelling radiance distribution.

The heart of RADS are two GE-2509 CID cameras. These cameras are 253V x 260H pixel cameras with the characteristics of low blooming (compared with CCD cameras)[10] and, as described later, a dynamic range of over 2 logs. These cameras allow on-chip integration to occur during frame periods through the use of injection inhibit. In this process the camera is not cleared between frame periods (the process of clearing is called injection)[10] thus the pixel array can accumulate charge over several frame increments enabling low light level images to be collected. This extends the maximum depth to which the camera system can operate.

A Poynting 509 frame grabber was used to convert the images to (eight bit) digital data. The frame grabber was repackaged and inserted into the underwater unit so that the analog video signal could be digitized at the source (camera) thus minimizing signal degradation. An RS-232, 9600 baud link was used between the frame grabber and the surface computer and all video data was all transferred up this digital link.

To obtain the surface incident radiance distribution a separate camera system was placed on deck in an active stable table. This system consisted of another GE-2509 camera, filter changer system, Poynting 509 camera controller (with a parallel computer interface versus the serial interface used in the underwater system), and an occulter to reduce the radiance from the sun to a manageable level. This deck system allowed the incoming radiance distribution to be measured and used both as input to radiative transfer models and to test for variations of incident flux during the underwater measurement. At the present time the surface data has not been reduced to radiometric form but has only been used to look at variations in the incident radiance field during the data casts.

A Hewlett Packard 310C microcomputer was used for overall instrument control and data reduction. The data was entered into this computer in byte form from the RS-232 data link and stored on a hard disk during data collection. For permanent archiving an Hewlett Packard 9144A 1/4" cartridge tape drive, with the capacity to store 182 megabytes data per cartridge, was used. The color CRT allowed data to be displayed on screen as false color images, or images could be sent to the surface camera controller and displayed in grey scale tones on a video monitor. A complete data package consists of two underwater images (upwelling and downwelling), and two surface images, a surface image taken before each underwater image.

4. DATA DISCUSSION

The images shown in Figure 3a-f were chosen to illustrate the change in the radiance distribution with depth. These show clearly the problem of ship shadow in measuring apparent optical properties, as the ship is the large square area on the left side of the downwelling image. The images were taken at 13:00 PDT on April 14,1987 at 33.033N, 118.217W, a position off of the San Diego coast and were all obtained with the 500 nm filter in place. These images have been reduced to radiance units(uW cm^{-2} nm^{-1} sr^{-1}), with the grey level showing the radiance levels and the position in the image determining the angular location of the given radiance level. The zenith angle is given by the radius position, while the azimuthal direction is indicated as the azimuthal angle on the image. The dark ring at between 40 and 50 degrees zenith in the downwelling radiance distribution is a region which we have blacked out because of questions about the data. This ring is the location of the edge of the neutral density coating on the window and there is overlap at the edge of this coating due to the finite aperture size of the fisheye lens. The grey levels in these images are on a scale in which each contour represents a range of 0.25 logarithmic units of radiance, with the grey colors repeating themselves every full log.

To reduce the effect of the missing data in the black ring, and also to fill in data at the edges of the image, a simple algorithm was developed. This algorithm uses a logarithmic least squares fit to the data between the ring and 5 degrees outside the ring and every 2.5 degrees in azimuthal angle, to extrapolate and fill the ring of missing data. The same overall procedure is used to fill the edges of the image out to 90 degrees, from the limit at 80 degrees which these images exhibited. An example of this process is shown in Figure 4a and 4b, where 4a is the original downwelling radiance distribution image and 4b is the reconstructed image. This procedure, while not exact, does seem to fill in the image reasonably well. The reconstructed images were used in calculating all of the apparent optical properties except the $K(r,\theta,\varphi)$ where the individual pixel values were considered too critical to approximate in this way, and no approximation was used.

Figure 5 shows the downwelling and upwelling scalar and vector irradiances calculated from the restored images shown in Figure 3 and other images of that cast (additional depths). The downwelling irradiances show a large ship shadow component in both the radiance distribution image and in the irradiance profiles. At positions deeper in the water column, the area of the ship shadow becomes a smaller portion of the radiance field sampled by the instrument which causes the irradiance to decrease less rapidly than would occur in the absence of the ship. This effect has been seen in other examples of irradiance data.

Figure 6 displays the average cosines derived from the irradiance data. The upwelling average cosine is very stable at a value of 0.4, while the downwelling average cosine remains around 0.9 (except at 60 meters where the downwelling average cosine falls to about 0.75).

The radiance attenuation coefficient $K(r,\theta,\varphi)$ was calculated for each pair of depths, where it was assumed that the incident radiance distribution did not vary appreciable between depth measurements of the cast. These values are displayed by two methods, the first is in Figure 7 where $K(r,\theta,\varphi)$ for 10 - 20 meters is displayed as an image in the same format as the radiance distribution images. The second format is the bar graphs in Figure 8a and Figure 8b. In the bar graphs, the percent occurrence of $K(r,\theta,\varphi)$ in a given range (0.01 m^{-1} range for the upwelling radiance attenuation and 0.02 m^{-1} for the downwelling radiance attenuation) is displayed versus the value of the radiance attenuation.

Values of beam attenuation versus depth indicated that the inherent property of c was not constant with depth -- the water was not homogeneous-- but instead had a c maximum at around 40 meters and a clearly defined layer of high c between 30 and 45 meters. If one investigates Figure 8a one sees that there are two trends in the distribution for $K(r,\theta,\varphi)$ values. The first is that the width of the distribution of values

narrows at greater depths; this is predictable from radiative transfer theory, in fact, if the water were homogeneous the distribution of values would slowly narrow until at the asymptotic depth the radiance attenuation became single valued. The second trend obvious in the data is the shifting of the peak of the distribution, due to the varying inherent properties of the medium.

Figure 8b illustrates that the downwelling radiance attenuation has the same trends as the upwelling radiance attenuation. A feature of the downwelling radiance attenuation is the significant number of negative $K(r,\theta,\varphi)$ values, implying an increase in the radiance distribution in these directions. These values occur in the region of the ship shadow, where the scattering tends to fill in the shadow, and the ship subtends a smaller solid angle of the radiance distribution at greater depths. This second effect causes some directions, which were looking at the dark area beneath the ship, to acquire an incident sky input. There are also some negative values in the 50 -60 meter distribution, and in fact the peak of the 50 - 60 meter value is lower than the predicted pure water KE_d,[11] this has not been resolved at the present time.

5. CONCLUSION

The change of the radiance distribution with depth has been illustrated for a single case. Other apparent optical properties, derived from the radiance distribution, have been presented. The radiance attenuation coefficient has been calculated, and its variation with depth illustrated. This parameter could be useful in verifying that the asymptotic depth has been reached, and indicates the change in radiance distribution with depth.

6. ACKNOWLEDGEMENT

This research has been supported under a contract from the Office of Naval Research, code 425. I would like to thank Mr. Roswell Austin for his support and ideas, and acknowledge the contributions of Mr. Richard Johnson in the filter changer ideas and construction. I would also like to thank Mr. Harry Sprink and Mr. Albert Chapin for their technical support, J.C. Brown for his graphical support, and Dr. Charles Trees for his review of the manuscript.

7. REFERENCES

1) K. J. Voss, "An underwater electro-optical radiance distribution camera system," submitted to Opt. Eng., Feb. 1988.

2) Standard Terminology on Optics of the Sea, I. A. P. S. O. Committee on Radiant Energy in the Sea, Goteborg, Sweden (1964).

3) R.C.Smith, R.W.Austin, and J.E.Tyler, "An Oceanographic Radiance Distribution Camera System," Appl.Opt.9, 2015-2022 (1970).

4) R.W.Preisendorfer, Hydrologic Optics, Vol. V, pp. 165-170, U.S. Dept. of Commerce, Hawaii (1976).

5) R. W. Preisendorfer, Model for radiance distribution in natural hydrosols, Visibility Lab, Scripps Institution of Oceanography, SIO Ref. 58-42, 1-15 (1957).

6) N. K. Hojerslev and J.R. Zaneveld, "A theoretical proof of the existence of the submarine asymptotic daylight field," Kobenhavns Universitet Instut for Fysisk Oceanografi, No. 34 (1977).

7) M.Herman and J. Lenoble, "Asymptotic radiation in a scattering and absorbing medium," J. Quant Spect. Rad. Transf. 8, 355-367 (1968).

8) R.W.Preisendorfer, Hydrologic Optics, Vol. 1, pp. 34-37, U.S. Dept. of Commerce, Hawaii, (1976).

9) K. Miyamoto, "Fish-eye lens," J. Opt. Soc. Am. 54, 1060-1061 (1964).

10) G.R.Sims and M.B.Denton, "Characterization of a charge-injection-device camera system as a multichannel spectroscopic detector," Opt. Eng. 26, 1008-1019 (1987).

11) R. C. Smith and K.S. Baker, Optical properties of the clearest natural waters," Appl. Opt. 15, 177-184 (1981).

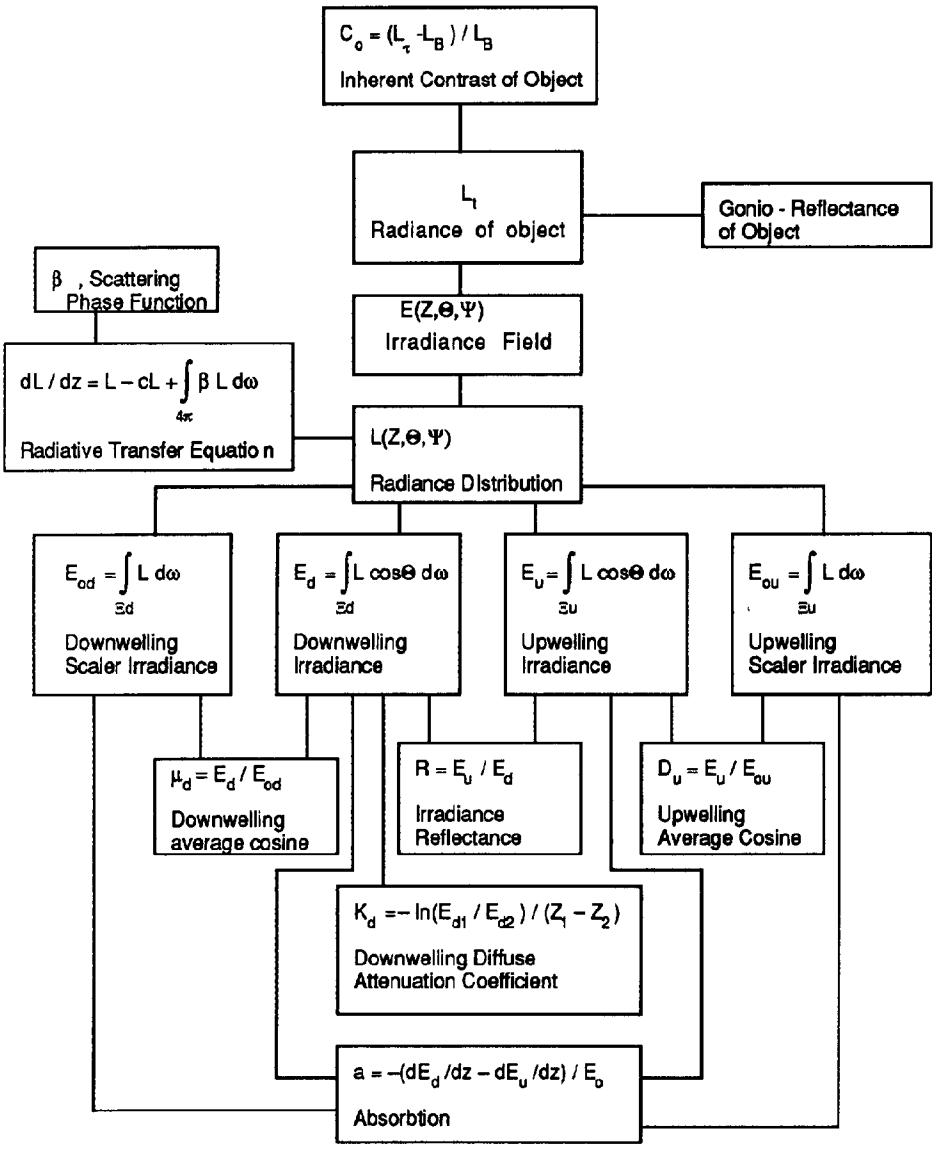

Figure 1. Chart of the connections between the radiance distribution and other apparent and inherent optical properties. (After Smith, Austin, and Tyler - Applied Optics, 9, 2015-2022(1970).

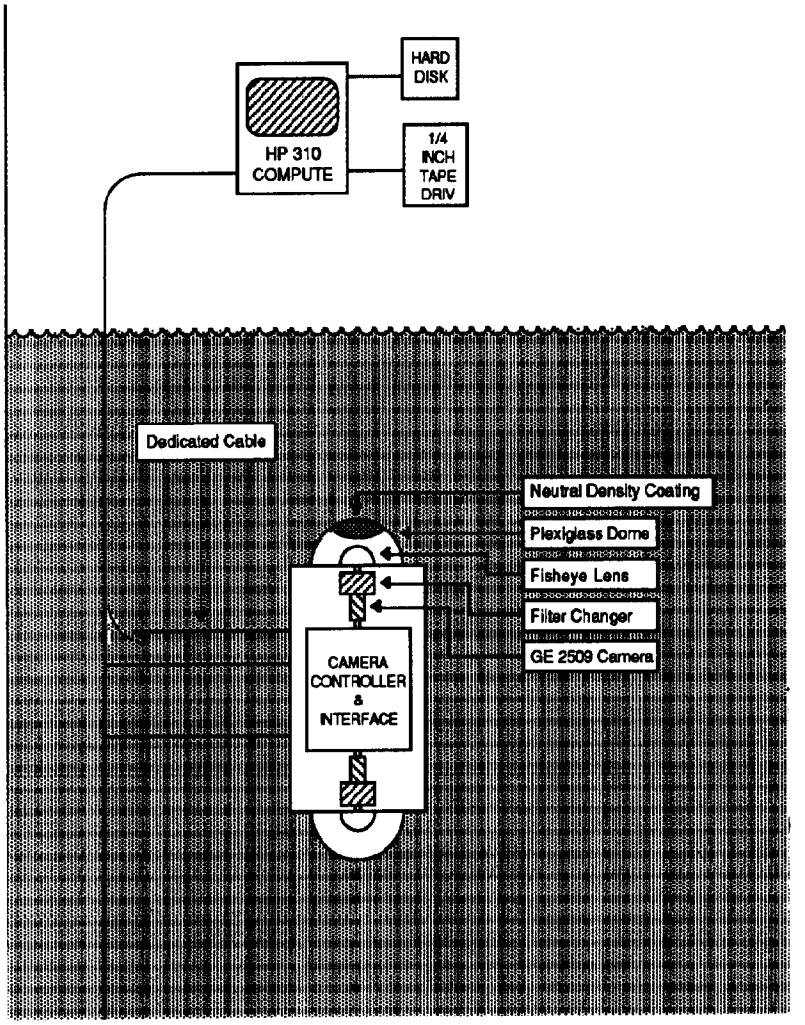

Figure 2. Stylized block diagram of Radiance distribution camera system.

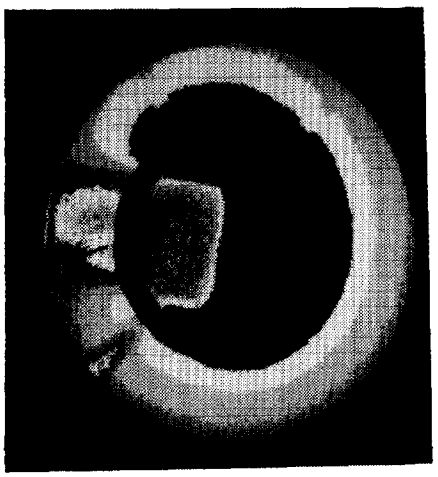

3a) Downwelling radiance distribution at 9.2 meters

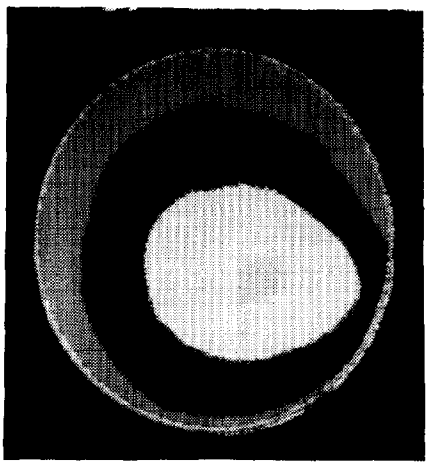

3b) upwelling radiance distribution as 9.2 meters

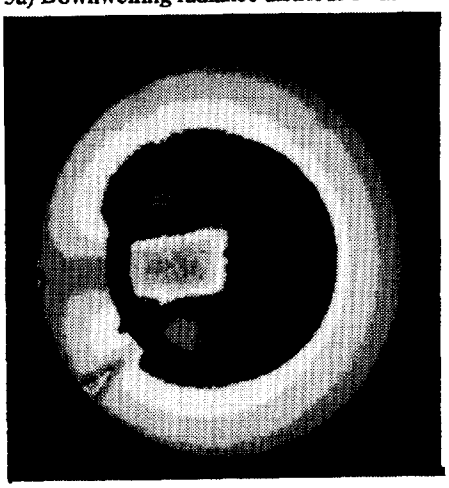

3c) downwelling radiance distribution at 20 meters

3d) upwelling radiance distribution at 20 meters

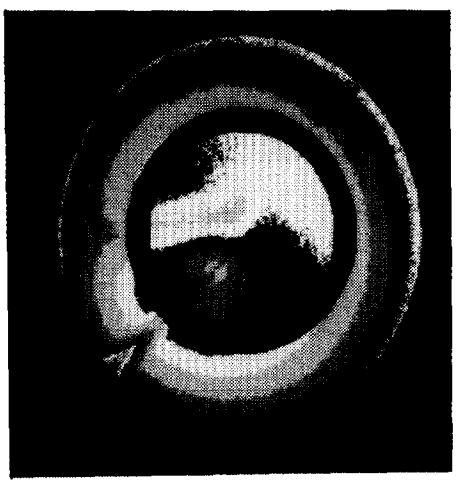

3e) downwelling radiance distribution at 30 meters

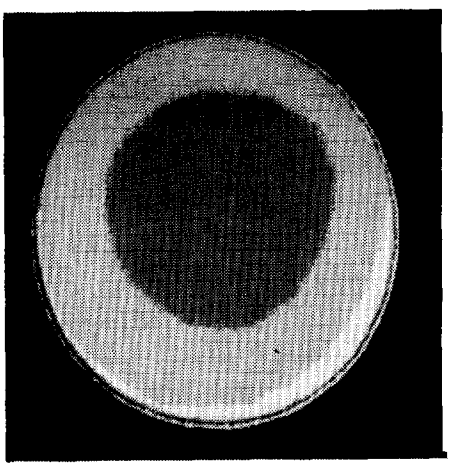

3f) upwelling radiance distribution at 30 meters

Figure 3a-f. Example images of the radiance distribution. All images were taken at approximately 13:00 PDT on April 14,1987 at 33.033N, 118.217W. Image format described in text.

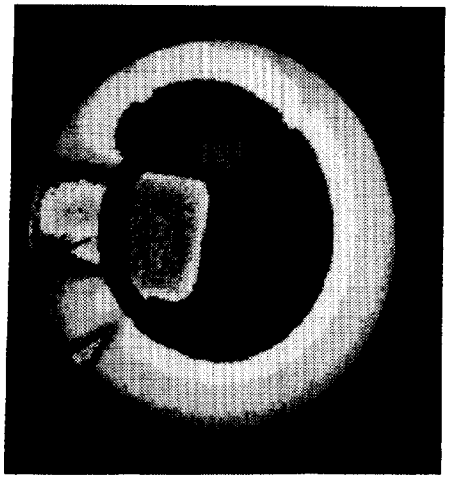

4a) original image, downwelling radiance distribution at 9.2 meters

4b) restored image, downwelling radiance distribution at 9.2 meters

Figure 4a-b. Example image showing result of image restoration.

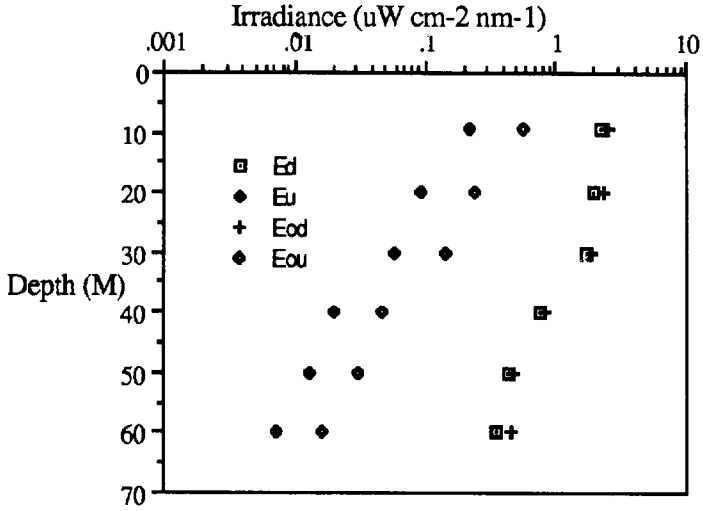

Figure 5. Plot of irradiance versus depth, irradiance values derived from radiance distribution images.

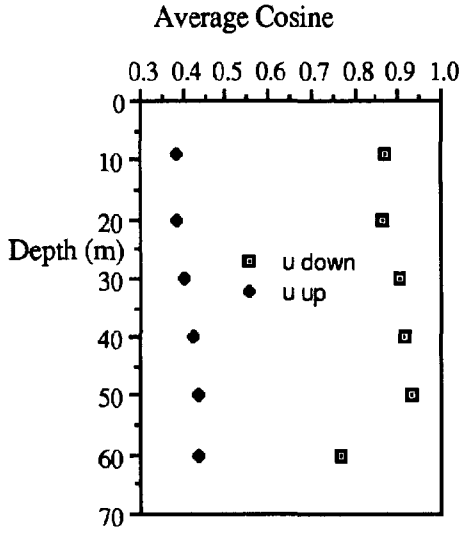

Figure 6. Plot of average cosine versus depth, derived from radiance distribution images.

Figure 7. Image of radiance attenuation for the depth interval 9.2 meters to 20 meters. Contours are values of equal radiance attenuation.

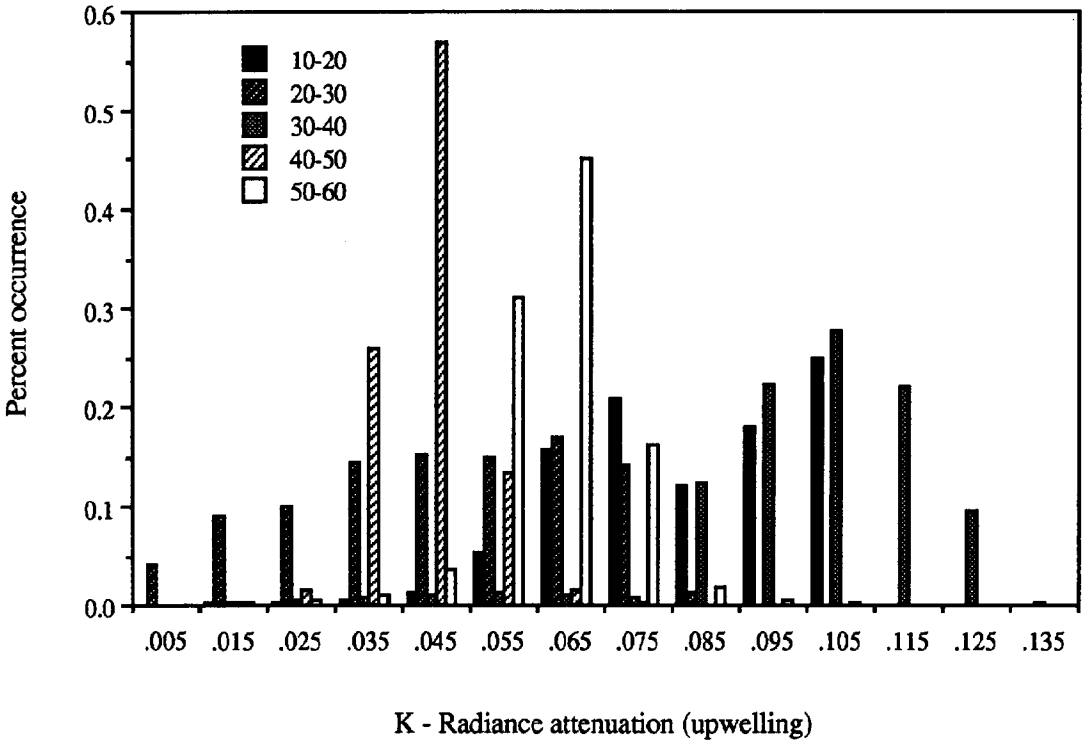

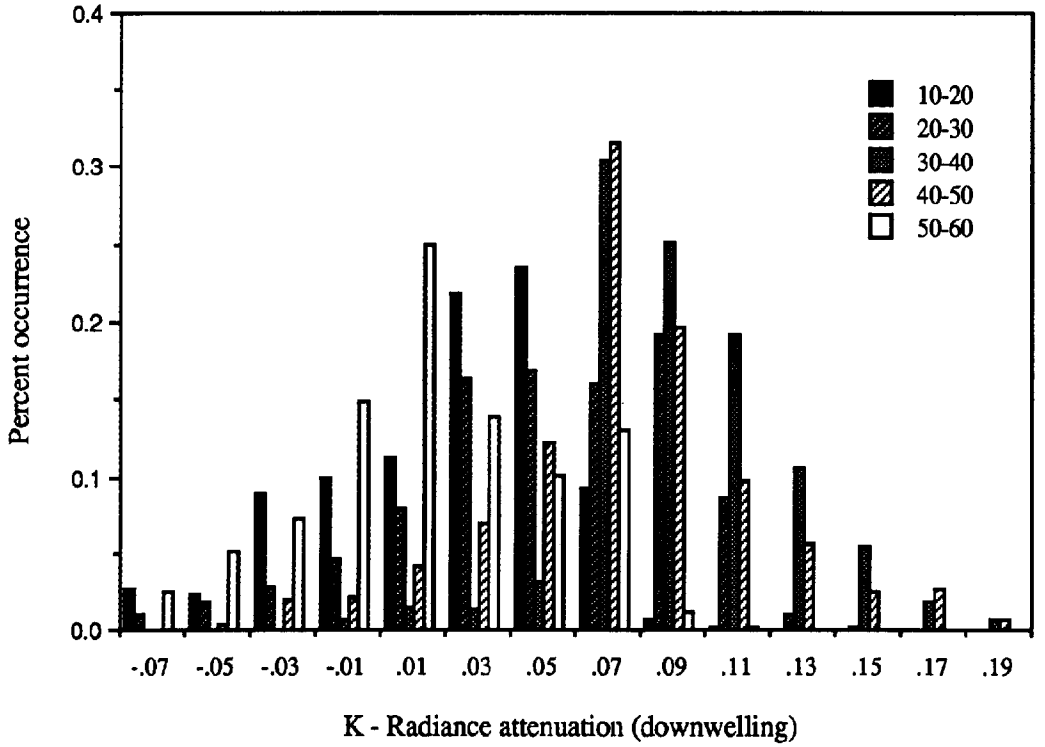

Figure 8a-b. Bar graphs illustrating the percent occurrence of values of radiance attenuation, for given depth intervals.